

## Accepted Manuscript

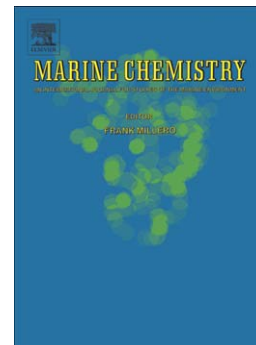
Radium Isotope Distributions during the US GEOTRACES North Atlantic Cruises

Matthew A. Charette, Paul J. Morris, Paul B. Henderson, Willard S. Moore

PII: S0304-4203(15)00003-1  
DOI: doi: [10.1016/j.marchem.2015.01.001](https://doi.org/10.1016/j.marchem.2015.01.001)  
Reference: MARCHE 3192

To appear in: *Marine Chemistry*

Received date: 26 September 2014  
Revised date: 23 December 2014  
Accepted date: 5 January 2015



Please cite this article as: Charette, Matthew A., Morris, Paul J., Henderson, Paul B., Moore, Willard S., Radium Isotope Distributions during the US GEOTRACES North Atlantic Cruises, *Marine Chemistry* (2015), doi: [10.1016/j.marchem.2015.01.001](https://doi.org/10.1016/j.marchem.2015.01.001)

This is a PDF file of an unedited manuscript that has been accepted for publication. As a service to our customers we are providing this early version of the manuscript. The manuscript will undergo copyediting, typesetting, and review of the resulting proof before it is published in its final form. Please note that during the production process errors may be discovered which could affect the content, and all legal disclaimers that apply to the journal pertain.

## Radium Isotope Distributions during the US GEOTRACES North Atlantic Cruises

Matthew A. Charette<sup>a\*</sup>, Paul J. Morris<sup>a†</sup>, Paul B. Henderson<sup>a</sup>, and Willard S. Moore<sup>b</sup>

<sup>a</sup>Department of Marine Chemistry and Geochemistry  
Woods Hole Oceanographic Institution  
Woods Hole, MA 02543 USA

<sup>b</sup>Department of Earth and Ocean Sciences  
University of South Carolina  
Columbia, SC 29208 USA

<sup>†</sup>Now at:  
Environment Laboratories  
Department of Nuclear Sciences and Applications  
International Atomic Energy Agency  
980000 Monaco  
Principality of Monaco

Submitted to *Marine Chemistry*, GEOTRACES Special Issue  
September 26, 2014

\*Corresponding author  
Email: mcharette@whoi.edu  
Tel: +1-508-289-3205

**Abstract**

Radium isotopes are produced in sediments via the decay of thorium isotopes and are generally soluble in seawater. As such, isotopes of the radium quartet ( $^{224}\text{Ra}$ ,  $^{223}\text{Ra}$ ,  $^{228}\text{Ra}$ ,  $^{226}\text{Ra}$ ) have been used as tracers of ocean boundary inputs and mixing processes. We measured radium isotopes on the US GEOTRACES North Atlantic cruises in 2010 and 2011, which crossed a number of key ocean boundary features including the Mediterranean outflow, the Mauritanian upwelling and oxygen minimum zones (OMZ) along western Africa, a hydrothermal plume over the mid-Atlantic Ridge (MAR), and the broad continental margin of the north-eastern United States. Radium isotope features at these locations are discussed in the context of their potential to quantify fluxes of trace elements and isotopes (TEIs) from common sources. Notable observations include: (1) a Mediterranean outflow spreading rate of 0.52-0.60 cm/s derived from  $^{228}\text{Ra}$ , (2) evidence of substantial sediment-water interaction in the benthic boundary layer along the OMZ, (3) decoupling between  $^{223}\text{Ra}$  and the other Ra isotope sources over the MAR, and (4) significant continental inputs (e.g. submarine groundwater discharge-SGD) in the western Atlantic. Lastly,  $^{228}\text{Ra}$  inventories have remained constant over the past 30 years, which suggests that SGD is steady-state for the North Atlantic on decadal time scales.

## 1. Introduction

Naturally occurring radium isotopes ( $^{226}\text{Ra}$ ,  $t_{1/2}=1600$  y;  $^{228}\text{Ra}$ ,  $t_{1/2}=5.75$  y;  $^{223}\text{Ra}$ ,  $t_{1/2}=11.4$  d;  $^{224}\text{Ra}$ ,  $t_{1/2}=3.66$  d) are produced *in situ* ubiquitously and continuously via decay of their parent thorium isotopes in sediments from the continental margin to the deep sea. Sediment porewater advective and diffusive mixing processes transport Ra isotopes from the sediments into the water column; once dissolved in seawater, they behave essentially conservatively. As such, they have been used for decades to quantify ocean mixing processes between shelf waters and the open ocean (Moore et al 1980; Moore et al 1985; Moore 1995), across the thermocline (Trier et al., 1972; Sarmiento et al., 1990), and in the benthic boundary layer over the abyssal plain (Sarmiento et al., 1982).

Historically, radium analyses were primarily restricted to the two longer-lived Ra isotopes,  $^{226}\text{Ra}$  and  $^{228}\text{Ra}$ , which limited the quantification of mixing processes to those occurring on time-scales of months to years. However, recent advances in sample collection coupled with on-board analysis of the short-lived Ra isotopes,  $^{224}\text{Ra}$  and  $^{223}\text{Ra}$ , have greatly expanded the power of these tracers to include mixing processes on time-scales of days to weeks (Moore and Arnold 1996; Moore 2000a and 2000b). In addition, streamlined processes for collection and analyses of the Ra quartet in the deep ocean (Henderson et al., 2013) allowed for their inclusion as part of the international GEOTRACES project, which has set out to “identify processes and quantify fluxes that control the distribution of trace elements and isotopes (TEIs) in the ocean and to establish the sensitivity of these distributions to changing environmental conditions”. Their inclusion in the program has been driven by the idea that measurements of the distribution of a stable trace metal alone, for example Fe or Al, no matter how accurate, are not sufficient for determining controlling processes or quantifying fluxes—a central goal of the GEOTRACES program.

Here we present an overview of Ra isotope distributions during the U.S. GEOTRACES North Atlantic survey. The Atlantic Ocean is relatively small and narrow and thus, even more so than other basins, lateral transport from ocean boundaries will affect TEI distributions. The chosen transect line was designed to intersect a wide range of biogeochemical regimes, with TEI distributions being controlled by, for example, (1) shelf-basin interactions including lateral input of intermediate and benthic nepheloid layers, (2) benthic inputs on the abyssal plain, (3) hydrothermal inputs and TEI scavenging associated with plume Fe and Mn (hydr)oxides, (4) oxygen minima in the shadow of an eastern boundary upwelling, (5) water mass mixing from major subbasin outflows, and (6) submarine groundwater discharge (SGD). Examples of how Ra isotopes can be used to better understand these various processes are the main focus of this paper.

## 2. Methods

The samples described herein were collected on the R/V *Knorr* during the U.S. GEOTRACES North Atlantic expedition (GEOTRACES GAO3). Originally scheduled to be completed in a single, two month cruise between Portugal and Woods Hole, the ship experienced propulsion problems after only three weeks so the cruise was split into two

legs. The 2010 leg (hereafter USGT10) was from Portugal to Cape Verde while the 2011 leg (USGT11) was from Woods Hole to Cape Verde.

### 2.1 Sample collection

The methods used for quantifying the four radium isotopes are described in detail by Henderson et al. (2013) and therefore are only briefly described here. Figure 1 is a flow chart that illustrates the sample collection, processing, and analytical procedures for Ra isotopes employed on the 2010 and 2011 U.S. GEOTRACES cruises. In short, the main sample collection system was a modified McLean in situ pump with dual filter heads and a single MnO<sub>2</sub> adsorber cartridge holder for scavenging dissolved (<1 μm) radium and thorium isotopes from seawater (Lam and Morris, pat. pending). The pump collection period was 4 hours at a setting of 8 L/min; depending on particle loading, sample sizes generally ranged from 1300-1700 L. At these flow rates, the MnO<sub>2</sub> cartridge does not have a 100% scavenging efficiency for Ra and Th; hence, small volume samples for <sup>226</sup>Ra (15-25 L) and <sup>234</sup>Th (4 L) were collected from a Niskin bottle mounted above the pump (>1000 m) or on a CTD rosette (<1000 m). The cartridge scavenging efficiency was determined from the ratio of <sup>226</sup>Ra and <sup>234</sup>Th on the cartridge relative to the small volume samples. Standard errors for the four radium isotopes were propagated from the counting error (gamma or RaDeCC) and the cartridge scavenging efficiency error. In the case of excess <sup>223</sup>Ra and <sup>224</sup>Ra, the error was propagated from the errors for total <sup>224</sup>Ra and <sup>228</sup>Th and total <sup>223</sup>Ra and <sup>227</sup>Ac, respectively.

### 2.2 Analysis of the short-lived Ra isotopes (<sup>223</sup>Ra and <sup>224</sup>Ra) by delayed coincidence counting

Cartridge samples were rinsed with deionized water (passed through an MnO<sub>2</sub> cartridge) and dried with filtered compressed air to remove excess moisture in preparation for analysis via delayed coincidence counting (RaDeCC; Moore and Arnold, 1996). Each sample was analyzed three times: ~36 hours, 4 weeks and 2 months post collection. The second and third analyses were used to determine the supported <sup>224</sup>Ra (from <sup>228</sup>Th) and <sup>223</sup>Ra (from <sup>227</sup>Ac), respectively. The first and second counting cycles consisted of up to two 180 min periods separated by a ~10 minute flushing of the counting cells to minimize build up of <sup>222</sup>Rn and its progenies, which can adversely affect the chance coincidence calculations for the <sup>224</sup>Ra daughter <sup>220</sup>Rn (Moore and Arnold, 1996). The third cycle was for ~20 hours with no flushing of the counting cell, since the chance coincidence corrections for <sup>219</sup>Rn are largely unaffected by <sup>222</sup>Rn buildup in the system.

The RaDeCC counters were calibrated with cartridges doped with <sup>226</sup>Ra, <sup>232</sup>Th, and <sup>227</sup>Ac standards (with daughters in secular equilibrium). Briefly, the cartridges were placed in 1-L plastic bags along with 300 ml of Ra-free seawater. The standard solutions were added to the bags and placed on a shaker table for 72 hours. The cartridges were air dried for 24 hours after which they were prepared for counting in the same manner as described above. The residual solution was passed through a MnO<sub>2</sub> acrylic fiber and analyzed for <sup>226</sup>Ra (via <sup>222</sup>Rn emanation) and RaDeCC, which indicated that >99.9% of the added tracers had sorbed to the cartridges.

### 2.3 Analysis of the long-lived Ra isotopes ( $^{226}\text{Ra}$ and $^{228}\text{Ra}$ ) by gamma counting

After the final RaDeCC analyses were completed, the cartridges were placed in ceramic coffee mugs, covered with a ceramic tile, and placed in a muffle furnace at  $820^\circ\text{C}$  for 48 hours. Ash weights typically ranged from 1.5 to 30 g with an average of 5.6 g. For weights greater than 10 g, the cartridge ash was transferred to 25 mm diameter polystyrene vials and sealed with epoxy (to prevent  $^{222}\text{Rn}$  loss); ash weights less than 10 g were transferred to 15 mm diameter vials. Samples were counted for 2-3 days in high purity, well-type germanium detectors to quantify  $^{226}\text{Ra}$  via the  $^{214}\text{Pb}$  photopeak at 352 keV and  $^{228}\text{Ra}$  via the  $^{228}\text{Ac}$  photopeak at 911 keV or by  $^{228}\text{Th}$  ingrowth as described below. The detectors were calibrated using ash prepared from cartridges soaked in a standard solution containing  $^{226}\text{Ra}$  and  $^{232}\text{Th}$  (with daughters in equilibrium).

### 2.4 Determination of $^{228}\text{Ra}$ via $^{228}\text{Th}$ ingrowth

Measurements of  $^{228}\text{Ra}$  by gamma spectrometry usually involve the  $^{228}\text{Ac}$  daughter peaks at 338 and 911 keV. However, these peaks have rather low intensities, 0.114 for the 338 keV peak and 0.277 for the 911 keV peak. Because of the decrease in detector efficiency (E) with increasing energy, the two peaks are rather similar in their effectiveness. Further down in the  $^{228}\text{Ra}$  decay chain is  $^{212}\text{Pb}$  at 238 keV, which has a 0.423 intensity (I). This is a much more effective peak because of the higher intensity and lower energy, albeit some gammas are lost by self absorption. Table 1 gives the relevant peak parameters for the University of South Carolina detector used to measure the GEOTRACES samples in an ashed  $\text{MnO}_2$  matrix at 25 mm height.

Here the Factor ( $1/(I \cdot E)$ ) is used to convert cpm to dpm (Moore 1984). Clearly the  $^{212}\text{Pb}$  peak has the lowest factor and is therefore the most effective peak. However, it is separated from  $^{228}\text{Ra}$  by  $^{228}\text{Th}$ , which has a 1.9 year half life. To use this peak we must know the initial activity of  $^{228}\text{Th}$  in the sample and wait until a new generation of  $^{228}\text{Th}$  is produced from  $^{228}\text{Ra}$  decay.

When  $^{228}\text{Ra}$  is extracted from sea water some  $^{228}\text{Th}$  is extracted as well. With time the relative amounts of  $^{228}\text{Ra}$  and  $^{228}\text{Th}$  (assuming no  $^{232}\text{Th}$  is present) will change as follows:

$$^{228}\text{Ra}_i = \frac{^{228}\text{Th}_m - \left[ ^{228}\text{Th}_i \exp(-\lambda_{\text{Th}} t) \right]}{1.499 \left[ \exp(-\lambda_{\text{Ra}} t) - \exp(-\lambda_{\text{Th}} t) \right]} \quad (1)$$

where  $^{228}\text{Ra}_i$  and  $^{228}\text{Th}_i$  are the initial activities of  $^{228}\text{Ra}$  and  $^{228}\text{Th}$  in the sample,  $^{228}\text{Th}_m$  is the measured  $^{228}\text{Th}$  after an elapsed time = t,  $\lambda_{\text{Ra}}$  and  $\lambda_{\text{Th}}$  are the decay constants of  $^{228}\text{Ra}$  and  $^{228}\text{Th}$ , respectively.

This equation has been used in conjunction with RaDeCC systems to measure  $^{228}\text{Ra}$  after elapsed times of 1-2 years (Moore 2008). The fibers are stored and recounted via

RaDeCC after the appropriate time has elapsed. We were not able to follow this simple procedure because we also wanted to measure  $^{234}\text{Th}$  on the fibers to estimate the fractional uptake of  $^{228}\text{Th}$ . In our procedure the fiber was ashed, then gamma counted for a short time to measure  $^{234}\text{Th}$ . Later the samples were gamma counted for a longer period (1-4 days) to measure the activity of  $^{228}\text{Ra}$  via the  $^{228}\text{Ac}$  peaks. Even with long counting periods some samples did not yield enough counts to produce a peak that could be quantified. However, in many of these cases a  $^{212}\text{Pb}$  peak could be resolved to estimate  $^{228}\text{Th}$ , which in turn could be used to calculate the initial  $^{228}\text{Ra}$  from equation 1. However, to achieve the best results, samples were recounted after about another year. In this case the initial  $^{228}\text{Th}$  had decreased by about half and a new generation of  $^{228}\text{Th}$  equivalent to about 45% of the initial  $^{228}\text{Ra}$  had grown in. These counts (~2 years post-collection) yield a  $^{212}\text{Pb}$  peak approximately 3-4 times stronger than the initial  $^{228}\text{Ac}$  peaks.

In almost all cases the counting error associated with the  $^{212}\text{Pb}$  peak is smaller than the one based on  $^{228}\text{Ac}$ . At station USGT10-1, the power of the  $^{212}\text{Pb}$  measurement is especially evident (Fig. 2). The  $^{228}\text{Ac}$  result for the 420 m sample is  $0.78\pm 0.13$  and for the 665 m sample it is  $1.06\pm 0.12$ , a difference of  $0.28\pm 0.18$ , but within 2-sigma. The  $^{212}\text{Pb}$  results for the same samples are  $0.36\pm 0.02$  and  $1.14\pm 0.08$ . Here the difference is  $0.78\pm 0.08$ , clearly beyond 3-sigma. The reason for the higher  $^{228}\text{Ra}$  in the deeper sample is recent outflow from the Mediterranean Sea as noted by the higher temperature and salinity at 665 m (see discussion in section 6). Herein we report the  $^{228}\text{Ra}$  activity from the method with the lowest counting uncertainty.

### 2.5 Analysis of small volume $^{226}\text{Ra}$ via $^{222}\text{Rn}$ emanation

Radium recovery on the cartridges was determined by comparing  $^{226}\text{Ra}$  in the cartridge ash with  $^{226}\text{Ra}$  on the small-volume Niskin bottle samples from the corresponding pump depth. The small volume samples (15-25 L) were gravity filtered ( $\sim 0.5\text{ L min}^{-1}$ ) through  $\sim 15\text{ g}$  of  $\text{MnO}_2$  acrylic fiber, which quantitatively removes Ra from seawater. The samples were rinsed with deionized water, partially dried, and placed in a sealed fiber-cartridge holder (Peterson et al., 2009). The fiber holder was flushed with He for 5 minutes at 250 ml/min, sealed, and held for a minimum of 5 days prior to analysis via  $^{222}\text{Rn}$  ingrowth and scintillation counting (Key et al., 1979). Samples were measured for 180 min, which typically resulted in counting uncertainties of 2-5%, dependent on sample volume and  $^{226}\text{Ra}$  content on the fiber. The method was standardized using NIST  $^{226}\text{Ra}$  (20 dpm) sorbed to  $\text{MnO}_2$  fiber and analyzed in the same manner as the samples. Standard reproducibility was 2-3% on average. Taking advantage of its well known oceanic relationship with barium (e.g. Chan et al., 1976) and silicate (e.g. Chung, 1980),  $^{226}\text{Ra}$  was compared against the Ba (Shiller, 2013) and Si distribution for the same stations and depths. This was used not only as an independent check on the quality of the data but also in limited cases to provide an estimate of  $^{226}\text{Ra}$  activity where a sample was missing due to an un-tripped Niskin bottle or for an outlier. Outliers were likely due to an incorrect record of sample volume or leaks/bypass of  $\text{MnO}_2$  fiber during filtration and were defined as a deviation of 30% or more from the predicted  $^{226}\text{Ra}$  based on the Ra/Si or Ra/Ba relationship. Two methods were used for  $^{226}\text{Ra}$  estimation in the case of a missing sample or outlier: (1) linear interpolation based on measured  $^{226}\text{Ra}$  activities above and below the

sample depth of interest (majority of cases) or (2) use of the  $^{226}\text{Ra}/\text{Ba}$  relationship (limited cases where sequential samples were not available due to un-tripped Niskin bottles). Regarding the latter, Chan et al. (1976) demonstrated the constancy of this relationship for samples collected in the Atlantic Ocean and the adjacent Arctic and Antarctic Oceans. They noted “that while there is a general tendency for the deep water to have lower ratios than the intermediate and bottom waters” the scatter in the data relative to the analytical uncertainty of 5% precluded a detailed interpretation. Hence, rather than separate the  $^{226}\text{Ra}/\text{Ba}$  data according to water mass, we used a single curve fit ( $R^2=0.91$ ) and assigned an uncertainty of 10% to such samples. According to the detailed data of Chan et al. (1976) this 10% uncertainty should account for potential differences due to water mass variability in the ratio. Data flags are provided for all the measurements and are detailed in the data archive available through the Biological and Chemical Oceanography Data Management Office (BCO-DMO) website (<http://www.bco-dmo.org/dataset/3846>).

### *2.6 Scavenging efficiency for Ra isotopes on MnO<sub>2</sub> impregnated acrylic cartridges*

Radium recoveries on the MnO<sub>2</sub> cartridges for the two Atlantic GEOTRACES cruises averaged  $52 \pm 22\%$  (standard deviation). As discussed previously by Henderson et al. (2013), we expected somewhat higher Ra preconcentration efficiencies based on a series of controlled experiments using these same cartridges in surface seawater. The experiments focused on the effect of flow rate through various Mn-coated media on Ra recovery and suggested that the CUNO acrylic MnO<sub>2</sub> cartridges were nearly 100% efficient at flow rates up to  $\sim 8 \text{ L min}^{-1}$ , but decreased significantly ( $\sim 30\%$ ) at flow rates  $>10 \text{ L min}^{-1}$ . Since we pumped at an average rate of  $\sim 6 \text{ L min}^{-1}$ , our average of 52% is difficult to explain since there was no clear controlling factor for variability in Ra recovery (e.g. Mn-content based on the weight of the ashed cartridges, water temperature, depth). However, since the cartridges were individually custom cut in half from single 10” cartridges, we cannot rule out water flow around poorly fitting cartridges as an explanation for the low Ra yield.

## *3. Results and Discussion*

### *3.1 Radium-226 relative to hydrographic features distributions*

The radium isotope data discussed herein are not listed in tabular form but are available for download through the BCO-DMO website (link provided above). Also, to aid in the interpretation of Ra isotope distributions, we frequently refer to a water mass analysis conducted by Jenkins et al. (2014), which was based on an Optimum Multi-parameter Analysis (OMPA) of several conservative oceanographic properties measured during the same GEOTRACES cruises.

The residence time of  $^{226}\text{Ra}$  in seawater is on the order of  $\sim 10^4$  years, though its mean life-time of 2300 years means that most  $^{226}\text{Ra}$  atoms will decay while resident in the ocean (Ku and Luo, 1994). While non-conservative behavior of the three shorter-lived Ra isotopes is not quantifiable in the open ocean relative to decay and mixing processes, such behavior can be observed for  $^{226}\text{Ra}$ . Surface waters of all ocean basins are slightly depleted in  $^{226}\text{Ra}$  due to uptake within planktonic Ca- and Si-based tests or co-precipitation with

barite ( $\text{BaSO}_4$ ) followed by export with sinking particles (Moore and Dymond, 1991; van Beek et al., 2007). Intermediate and deep water are enriched above surface values due to a combination of particle remineralization (Broecker et al., 1976) and diffusion from sediments (Cochran, 1980); hence,  $^{226}\text{Ra}$  displays a nutrient type distribution in the ocean with higher values in the deep Pacific relative to the Atlantic corresponding to an increase in deep water age (Broecker et al., 1967; Chung, 1980).

Radium-226 sections for the North Atlantic GEOTRACES cruises are shown in Figure 3 (cruise station numbers are also found in this figure). Surface activities are relatively constant at between 8-9 dpm/100 L across both sections, consistent with previously reported  $^{226}\text{Ra}$  values for this ocean basin (Broecker et al., 1976). A terrestrial  $^{226}\text{Ra}$  source is only observed for the two innermost stations along the mid Atlantic Bight (~10-15% enrichment above open ocean values), near where Moore (1996) attributed elevated  $^{226}\text{Ra}$  activities to input via submarine groundwater discharge.

Subsurface  $^{226}\text{Ra}$  activities are generally lower to the west of the mid Atlantic Ridge (MAR) corresponding to the lower age of the deep water found there. Specifically, the western basin subsurface is dominated by recently ventilated North Atlantic Deep Water masses including Labrador Sea Water (~1000-3000 m; 10-12 dpm/100 L) and Iceland Scotland Overflow Water (ISOW; >3000 m; 12-16 dpm/100 L; Jenkins et al., 2014). Evidence for Antarctic Bottom Water (AABW) is observed in the deep (>5000 m) western basin (station USGT11-12), with  $^{226}\text{Ra}$  activities in excess of 18 dpm/100 L. At 5100 m, for example, the OMPA of Jenkins et al. (2014) indicates the presence of 40% AABW with the balance supplied by various contributors to North Atlantic Deep Water (NADW). If NADW contains at most 12 dpm/100 L  $^{226}\text{Ra}$  and the AABW source is 23 dpm/100 L (Ku and Lin, 1976), then simple two endmember mixing would suggest that the AABW component is closer to 65%. Since the recently ventilated NADW  $^{226}\text{Ra}$  endmember cannot be significantly higher and the AABW activity is well constrained, an additional  $^{226}\text{Ra}$  source equivalent to ~7 dpm/100 L is required to explain the discrepancy. Possible sources include  $^{226}\text{Ra}$  diffusion from bottom sediments or biogenic recycling of particulate  $^{226}\text{Ra}$ . If the transit time for AABW to 30°N is ~100 y (Broecker, 1979) and the excess  $^{226}\text{Ra}$  is distributed over the lower 500 m of the water column, then the  $^{226}\text{Ra}$  flux required to balance the excess is ~350 dpm/m<sup>2</sup> y. Cochran (1980) found an inverse correlation between sediment  $^{226}\text{Ra}$  flux and sedimentation rate. As such, the productive Atlantic Ocean had the lowest sedimentary  $^{226}\text{Ra}$  fluxes, which ranged from 15-22 dpm/m<sup>2</sup> y, nearly two orders of magnitude lower than North Pacific Ocean sediments. Since the sediment flux is only ~5% of the total flux required to explain  $^{226}\text{Ra}$  excess, particle regeneration must supply the majority of deep water  $^{226}\text{Ra}$  in the Atlantic Ocean (Broecker et al., 1976; Chan et al., 1976). This process is also responsible for enriched Si and Ba at depth in the North Atlantic (Chan et al., 1976).

To the east of the MAR, the AABW  $^{226}\text{Ra}$  signature is even stronger (18-21 dpm/100 L), extending from ~3000 m to the seafloor. These GEOTRACES sections suggest that the water column between 1000-3000 m is a mixture of  $^{226}\text{Ra}$  rich Antarctic Intermediate Water (AIW)/Upper Circumpolar Deep Water (UCDW) and  $^{226}\text{Ra}$  poor Labrador Seawater (LSW), which results in the intermediate  $^{226}\text{Ra}$  values observed here (12-16 dpm/100 L).

At the southern end of the meridional transect,  $^{226}\text{Ra}$  activities indicative of the same water mass features observed to the west of the MAR were generally present (in order of increasing depth below 1000 m): AIW, UCDW, LSW, and AABW. At the northern end, low  $^{226}\text{Ra}$  activities (8-10 dpm/100 L) between ~600-2000 m that are indistinguishable from surface water are associated with the Mediterranean Outflow Water (MOW; Schmidt and Reys, 1996; Jenkins et al., 2014).

While the coupling between the ocean  $^{226}\text{Ra}$  and silicate cycles has been well established, the relationship between the two in the North Atlantic is somewhat unique. The  $^{226}\text{Ra}/\text{Si}$  ratio (units of  $10^3$  dpm/mol) typically ranges from 0.8 for the circumpolar region (Ku and Lin, 1976; Chung, 1980) to 1.9 for the central North Pacific (Chung, 1980). For the North Atlantic however,  $^{226}\text{Ra}/\text{Si}$  ranges from 2.1 for the mean water column) to 2.4 for samples excluding the upper ocean (defined as  $\text{Si} > 5\mu\text{M}$ ; Fig. 4). This is a result of mixing between NADW, which is recently ventilated and therefore is depleted in Si but composed of  $^{226}\text{Ra}$  activities near those of typical surface water (i.e. high  $^{226}\text{Ra}/\text{Si}$ ), and the two main circumpolar sources (AABW and AIW) with lower  $^{226}\text{Ra}/\text{Si}$  ratios (Broecker et al., 1967).

### 3.2 Controls on $^{228}\text{Ra}$ distributions in the North Atlantic

The main source of  $^{228}\text{Ra}$  in the ocean is from  $^{232}\text{Th}$  decay in sediments and subsequent exchange between sediment porewater and the overlying water column (Moore, 1969; Kaufman et al., 1973). Combined with its relatively short half-life with respect to ocean-basin scale mixing processes, its presence in seawater is indicative of recent (~years-decades) contact with ocean boundaries such as continental shelves and pelagic sediments (Sarmiento et al., 1982; Hammond et al., 1990). Furthermore, though it has been used as a tracer of particle source in the mesopelagic (van Beek et al., 2006), unlike  $^{226}\text{Ra}$ , rates of particle uptake and remineralization are small relative to  $^{228}\text{Ra}$  input and decay.

A section plot for  $^{228}\text{Ra}$  is shown in Figure 5. In the surface ocean along the zonal transect,  $^{228}\text{Ra}$  activities are significantly higher in the western basin (4-8 dpm/100 L vs. 2.5-4 dpm/100 L). This is due to the large SGD-derived Ra source along the eastern coast of the United States (Moore et al., 2008). Minimum surface values of 2.5-3 dpm/100 L, generally centered over the MAR, are due to mixing and decay during transit away from the boundary source. Penetration of  $^{228}\text{Ra}$  into the thermocline is largely driven by mixing processes (Moore, 1972; Trier et al., 1972), and density gradients retard mixing. Hence, the maximum upper ocean  $^{228}\text{Ra}$  activities are well correlated with potential temperature (Fig. 5), the nutricline (not shown), and the distribution of North Atlantic Central Water (NACW; Jenkins et al., 2014). The NACW extends to 600 m through most of the western basin, but shoals to the east as it is displaced by Atlantic Equatorial Water (AEW; Jenkins et al., 2014). This feature, combined with upwelling off West Africa results in sharper  $^{228}\text{Ra}$  gradients and low  $^{228}\text{Ra}$  activities as shallow as 200 m. In the thermocline waters of the meridional transect,  $^{228}\text{Ra}$  activities largely mirror those of the east-west transect with  $^{228}\text{Ra}$  penetration extending to 400 m to the north while shoaling to <200 m in the south. This

distribution is consistent with the NACW and AEW water masses identified by the OMPA (Jenkins et al., 2014).

In the intermediate waters at USGT10-1, the MOW influence imparts an anomalous mid-water column  $^{228}\text{Ra}$  enrichment obtained from enhanced sediment-water interaction as MOW exits the Straits of Gibraltar (Schmidt and Reys, 1996). This feature extends southward to USGT10-3 and is discussed in more detail below. Elsewhere, mid-water column anomalies in  $^{228}\text{Ra}$  are generally restricted to the western and eastern basin ocean margins, where activities rarely fall below 0.5 dpm/100 L regardless of depth. These subsurface enrichments are likely due to sediment-water interaction and transport along isopycnal surfaces (Sarmiento et al., 1982).

Near-bottom  $^{228}\text{Ra}$  activities are generally in the range of 0.5-1 dpm/100 L, with higher values at the western and eastern ends of the transect and along the full length of the meridional transect, which follows the eastern boundary of the North Atlantic. One exception is offshore of Mauritania (USGT10-9), where benthic  $^{228}\text{Ra}$  activities are in excess of 3 dpm/100 L. This region receives among the highest dust fluxes in the global ocean (Jickells et al., 2005; Measures et al., 2014) and we surmise that the underlying sediments are rich in terrestrially-derived  $^{232}\text{Th}$ . In addition, upwelling in this region supports high biological productivity and export production. The associated accumulation of organic matter in the shelf/slope sediments leads to strong reducing conditions in the sediments and remobilization of Fe and Mn from sediments into the overlying water column. Together, these processes likely explain the co-occurrence of the highest near bottom  $^{228}\text{Ra}$  activities and dissolved Mn concentrations recorded during the U.S. GEOTRACES cruises (Hatta et al., 2014).

### *3.3 Ra isotopes at the TAG hydrothermal vent field*

Early work on radium in hydrothermal systems focused on ratios in high temperature fluids as a means to derive their residence time in the crust (Turekian and Cochran 1986; Kadko and Moore 1988). Other studies used Ra and Th/Ra activity ratios in active and inactive vent chimneys to glean information on both the duration and age of active venting (Stakes and Moore 1991). However, at present, no data exists on the radium isotope systematics within large-scale hydrothermal plumes despite the fact that like  $^3\text{He}$ , radium is highly enriched in high temperature fluids (Krishnaswami and Turekian, 1982; Kadko, 1996) and may be detected many 100s of kilometers downstream of active ridge crests.

The TAG hydrothermal vent field (Rona et al., 1984) neutrally buoyant plume was successfully sampled at station USGT11-16. Both  $^{226}\text{Ra}$  and  $^{228}\text{Ra}$  display maxima at 3400 m, approximately 280 m from the seafloor (Fig. 6). Peak activities are 16.5 and 0.40 dpm/100 L, respectively. These maxima are slightly deeper than other geochemical indicators of the hydrothermal plume such as  $^3\text{He}$  (Jenkins et al., 2014), Ba (Shiller, 2013), and dissolved trace metals (Fe, Mn, Al; Hatta et al., 2014), due to either cast-to-cast variability in plume height or that the lower resolution pumping casts (16 vs. 24 depths per station) may not have captured the true core of the plume. Furthermore, the signature of

the Ra-enriched hydrothermal-fluid has clearly been dispersed to a certain extent vertically. Near bottom  $^{226}\text{Ra}$  activities are 14.2 dpm/100 L; compared with this background value, the  $^{226}\text{Ra}$  enrichment is relatively low, but consistent with the expected rapid dilution of hydrothermal fluids upon mixing with seawater (Rudnicki and Elderfield, 1992). The  $^{228}\text{Ra}$  enrichment is less obvious due to a near bottom increase from sediment  $^{228}\text{Ra}$  diffusion, but of the same order of magnitude as  $^{226}\text{Ra}$  (0.35 vs. 0.40 dpm/100L or ~13%). There is also evidence of the hydrothermal plume in the form of enriched mid-water column  $^{228}\text{Ra}$  (2500 m) to the west of the ridge crest (USGT11-14; Fig. 5); this was also evident from the distribution of a number of other TEIs with a strong hydrothermal source (e.g. Jenkins et al., 2014b; Hayes et al., 2014; Measures et al., 2014).

### 3.4 Comparison with historical open ocean radium isotope distributions

There are a number of historical Ra isotope data sets with coverage in the North Atlantic, which allow for a comparison with our GEOTRACES results. Schmidt and Reys (1996) used  $^{228}\text{Ra}$  as a tracer of Mediterranean Outflow Water during two cruises in 1989 with a focus on two MOW eddies due west (500-1000 km) of the Straits of Gibraltar (Fig. 7e). The signature hydrographic characteristics of MOW are subsurface (~500-1500 m) peaks in both salinity and temperature. Schmidt and Reys (1996) reported subsurface maxima in  $^{228}\text{Ra}$  (eddy Nicole: 0.93 dpm/100 L; eddy Yseult: 0.83 dpm/100 L) associated with peaks subsurface salinity (36.457 and 36.122 for Nicole and Yseult, respectively) within both eddies. Station USGT10-3 is the closest proximal station to the earlier study stations, though USGT10-1 contains the least diluted MOW signature according to the water mass analysis of Jenkins et al. (2014) (Fig. 7d). Indeed, USGT10-1 has the highest  $^{228}\text{Ra}$  in the MOW region (0.82-1.4 dpm/100 L; Fig. 7c) with activities slightly above but consistent with the MOW  $^{228}\text{Ra}$  anomalies observed in 1989. In addition to  $^{228}\text{Ra}$ ,  $^{226}\text{Ra}$  is slightly elevated in the MOW (Fig. 7b) at USGT10-1 and approximately 10-20% higher than the  $^{226}\text{Ra}$  in MOW from 1989 (not shown). Aside from the MOW-related Ra isotope anomalies, the surface  $^{226}\text{Ra}$  and  $^{228}\text{Ra}$  are highly enriched compared with the historical data ( $^{226}\text{Ra}$ : ~9 vs. 6 dpm/100 L;  $^{228}\text{Ra}$ : ~2-3 vs. 1 dpm/100 L), suggesting a greater degree of coastal influence in this region of the North Atlantic at the time of the GEOTRACES cruise.

While sediment-water interaction imparts  $^{228}\text{Ra}$  on MOW as it transits the Straits, transport time and mixing will determine the  $^{228}\text{Ra}$  activity as MOW propagates through the North Atlantic basin. USGT10-1 had the highest  $^{228}\text{Ra}$  activity at 1.4 dpm/100 L within the MOW plume, consistent with the OMPA-derived MOW fraction of 94-100% within the same depth horizon (Fig. 7d). Peak  $^{228}\text{Ra}$  values at USGT10-3 were only ~0.45 dpm/100 L, slightly lower than the nearby historical station (0.7-0.9 dpm/100 L). If we assume that the USGT10-1  $^{228}\text{Ra}$  activity at 665 m is equivalent to the MOW endmember (1.4 dpm/100 L), then we can calculate the advection velocity of the MOW into the North Atlantic Ocean through comparison with dilution-corrected  $^{228}\text{Ra}$  activity at the same density horizon at USGT10-3 (775 m). Assuming no  $^{228}\text{Ra}$  contribution from outside the plume at this depth and a MOW fraction of 64% (Fig. 7d, Jenkins et al., 2014), the dilution corrected  $^{228}\text{Ra}$  activity is 0.701 dpm/100 L compared with 1.4 dpm/100 L at the source. This implies a transit time of one  $^{228}\text{Ra}$  half-life (~6 years) between the Straits of Gibraltar and USGT10-3

located ~1000 km to the west or ~0.60 cm/s. A similar analysis for samples closer to the lower boundary of the MOW plume (1000 m) yields a velocity of ~0.52 cm/s. These estimates are consistent with a theoretical estimate of 0.55 cm/s for the mean southward motion of MOW (de Verdier, 1992), but significantly slower than MOW transported via eddies (~3 cm/s; Armi et al., 1989).

The GEOSECS and Transient Tracers in the Ocean (TTO) programs both included measurement of the two long-lived Ra isotopes. The GEOSECS North Atlantic test station (Aug. 1970; 35.8°W, 68°W; Trier et al., 1972) and TTO station 6 (Apr. 1981; 34.7°N, 67.4°W; Key et al., 1990, 1992a,b) are the closest historical stations to USGT11-8 (Nov. 2011; 35.4°N, 66.7°W). For  $^{226}\text{Ra}$ , the three profiles are quite similar except for the upper 400 m of the GEOSECS data where activities range from 7-7.4 dpm/100 L compared with 8.1-8.7 dpm/100 L for TTO and GEOTRACES (Fig. 8b). However, Chung et al. (1974) compiled  $^{226}\text{Ra}$  data from multiple labs at the same station and found that the earlier upper ocean results were systematically lower by 20%. Hence, subsequent GEOSECS data from the same location are consistent with TTO and GEOTRACES  $^{226}\text{Ra}$  water column distributions. We further compared TTO and GEOTRACES  $^{226}\text{Ra}$  distributions by comparing the water column inventories (full ocean depth) from 15° x 15° boxes through the North Atlantic (Table 2). The agreement is excellent, with the highest divergence between the two datasets for an individual box being less than 5%, and the total inventory across all boxes agreeing to within 1%. These results not only validate the quality of the GEOTRACES  $^{226}\text{Ra}$  data, but also imply that ocean  $^{226}\text{Ra}$  sources and sinks (at least for the North Atlantic) are in steady state on a time scale of ~30 years.

There is also good agreement between  $^{228}\text{Ra}$  for the three datasets (Fig. 8c). Surface  $^{228}\text{Ra}$  activities range from ~3.7-4.5 dpm/100 L, near background values are present between ~2000-4000 m, and near bottom activities increase to ~1 dpm/100 L. Higher  $^{228}\text{Ra}$  activities are seen in the older profiles at 500 m and between 3000-4500 m, which might be attributed to subsurface horizontal advection of  $^{228}\text{Ra}$  from the ocean margin along constant density surfaces (Sarmiento et al., 1982; Charette et al., 2007). Alternatively, the radium samples collected on the GEOSECS cruise were collected with large volume Niskin bags or Gerard bottles, which showed evidence (from salinity) of leakage of  $^{228}\text{Ra}$ -rich near-surface water into the samplers (Trier et al., 1972). The deep-water data were not corrected for this  $^{228}\text{Ra}$  “blank” since the extent of the problem was not entirely known. The possible bottle leakage issue for the GEOSECS profile only impacts the  $^{228}\text{Ra}$  distribution since mid-water column activities are low relative to surface water (unlike  $^{226}\text{Ra}$ ).

### *3.5 Using Radium-228 inventories to quantify submarine groundwater discharge*

The inventory of  $^{228}\text{Ra}$  in the upper Atlantic has been used to estimate the total flux of submarine groundwater discharge to the Atlantic Ocean (Moore et al., 2008). We present a brief summary of this technique. The authors assumed that  $^{228}\text{Ra}$  was in steady state in the upper Atlantic, thus the total flux of  $^{228}\text{Ra}$  would be equivalent to the amount that decayed each year plus a small fraction (~1%) removed on particles via the biological

pump. Using data obtained during the TTO project, 1981-1986, the authors constructed a map of  $^{228}\text{Ra}$  inventories ( $\text{dpm m}^{-2}$ ) for the entire Atlantic. They grouped the data from each station (0 to 1000 m) into  $15^\circ \times 15^\circ$  boxes and averaged all stations in each box to obtain a box average. They then averaged all boxes to obtain a grand average and multiplied this by the surface area of the Atlantic to obtain the total inventory of  $^{228}\text{Ra}$  in the upper 1000 m. This inventory has recently been confirmed by Kwon et al. (2014) who used the TTO  $^{228}\text{Ra}$  data set in conjunction with a global ocean circulation model in which the ocean circulation field was constrained by observed temperature, salinity, radiocarbon, Chlorofluorocarbon-11, sea surface height and air-sea exchange of heat and freshwater fluxes. The inventory of  $^{228}\text{Ra}$  defines its steady state flux ( $\text{Flux} = \text{Inventory} \times \text{decay constant}$ ). Moore et al (2008) then estimated the fluxes of  $^{228}\text{Ra}$  from (1) rivers, including desorption from suspended particles, (2) diffusion from continental shelf and slope sediments, including the effects of bioturbation and irrigation, and (3) desorption from atmospheric dust. The sum of these fluxes was less than half the required input flux of  $^{228}\text{Ra}$ . They attributed the missing flux to SGD. Using data from groundwater samples collected along the Atlantic coast, they estimated the volume of SGD required to balance the missing  $^{228}\text{Ra}$  flux. A significant conclusion of this study was that the volume of SGD entering the Atlantic was similar to the volume of river water. They clearly emphasized that this was not a flux of fresh water, but rather a mixture of fresh and salty groundwater with unknown salinity.

A key assumption in the Moore et al. (2008) study was that  $^{228}\text{Ra}$  is in steady state in the upper Atlantic. Without this assumption, there would be no way to derive the total flux of  $^{228}\text{Ra}$ . Virtually all ( $\sim 95\%$ ) of the  $^{228}\text{Ra}$  present in the ocean during TTO has now decayed. Radium samples collected on the USGT10 and USGT11 cruises provide an opportunity to compare the data sets to determine if the steady state assumption is valid. These sections comprise a large swath of the central North Atlantic where some of the highest  $^{228}\text{Ra}$  inventories were measured during TTO.

We used the same technique used by Moore et al. (2008) to estimate the inventory of  $^{228}\text{Ra}$  in each  $15^\circ \times 15^\circ$  box from  $15^\circ$ -  $45^\circ\text{N}$  across the Atlantic to 1 km depth. The comparison of the TTO and GEOTRACES inventories are shown in Figure 9. The agreement within individual boxes is very good; the overall average of data in 6 boxes agrees within  $\pm 7\%$ , similar to the errors on the measurements (Table 3). Most boxes contain several stations, the exception being the box just west of Portugal and Gibraltar, where GEOTRACES had only one station. This station (Station 1) sampled a distinct subsurface plume of high salinity Mediterranean water containing elevated  $^{228}\text{Ra}$  activities compared to samples from other stations at this depth. Thus, the GEOTRACES average for this box is not representative. TTO had 3 stations in this box, so the Mediterranean influence was significantly diminished. If we exclude this box from the grand average, the TTO and GEOTRACES inventories for 5 boxes agree to within 2% (Table 3). We take this as strong evidence that  $^{228}\text{Ra}$  has been at steady state during the past 3 decades; thus, the estimate of the SGD flux based on this assumption is valid.

### *3.6 Short-lived Ra isotopes in the open ocean*

All GEOTRACES samples underwent an initial RaDeCC analysis immediately after collection onboard the ship, which allows us to report the first data on deep ocean short-lived Ra isotopes. Given their half-lives,  $^{223}\text{Ra}$  and  $^{224}\text{Ra}$  allow for quantification of mixing processes on time-scales of  $\sim 2$  months and  $\sim 3$  weeks, respectively. Hence, they will only be detected within a relatively short distance from the source: typically 10-100 km from a coastline in the surface mixed layer or 10-100 m from the sediment-water interface over the abyssal plain. Furthermore, in the coastal ocean the short-lived Ra isotope activities are largely unsupported via parent isotope decay. In the abyssal ocean, however, water column  $^{228}\text{Th}$  and  $^{227}\text{Ac}$  can support a large fraction of the measured  $^{224}\text{Ra}$  and  $^{223}\text{Ra}$ , respectively. Hence, the vast majority of our samples are below detection for the “excess” or unsupported activities of these two Ra isotopes. Here, since Moore (2000a,b) and others have reported surface ocean transects for  $^{223}\text{Ra}$  and  $^{224}\text{Ra}$ , we focus on near bottom examples from the GEOTRACES dataset.

As previously noted, station USGT10-9 displayed an unusually high  $^{228}\text{Ra}$  enrichment in the bottom boundary layer. The same is true for  $^{223}\text{Ra}$  and  $^{224}\text{Ra}$  (Fig. 10; reported as the excess Ra isotope [ $\text{Ra}_{\text{XS}}$ ] activity not supported by decay of their parent isotopes). The deepest sample, which is located approximately 50 m above the seafloor, contained a  $^{224}\text{Ra}_{\text{XS}}$  activity of 0.71 dpm/100 L and a  $^{223}\text{Ra}_{\text{XS}}$  activity of 0.13 dpm/100 L. For both isotopes, activities decrease sharply for the initial 100 m above the seabed, then somewhat linearly from 2900 m to 1250 m. The former distribution fits the expected pattern for isotope decay during diapycnal mixing, whereas the latter might be indicative of vertical water mass advection (i.e. upwelling). However, since there is a density gradient across this depth range, we can explain this contradiction via lateral Ra input along isopycnal surfaces from slope sediments given the very close proximity of USGT10-9 to the coastline.

As noted previously, the hydrothermal station (USGT11-16) included measurable  $^{226}\text{Ra}$  and  $^{228}\text{Ra}$  anomalies associated with the neutrally buoyant plume. However, while there is also clearly an anomaly in  $^{224}\text{Ra}_{\text{XS}}$  centered on 3400 m, peak activities in  $^{223}\text{Ra}_{\text{XS}}$  are associated with the deepest sample located at 3600 m ( $\sim 80$  m above the ridge crest; Fig. 6c). Hence, there appears to be a strong bottom source of  $^{223}\text{Ra}_{\text{XS}}$  that is obscuring  $^{223}\text{Ra}_{\text{XS}}$  being supplied by the plume. Notably, the  $^{223}\text{Ra}_{\text{XS}}$  activity in the bottom most sample is 0.97 dpm/100 L while  $^{224}\text{Ra}_{\text{XS}}$  is significantly lower at 0.16 dpm/100 L. Crustal activity ratios of the short-lived Ra isotope parents ( $^{235}\text{U}$ : $^{232}\text{Th}$ ) are typically 0.05 (Rama and Moore, 1996), similar to the  $^{223}\text{Ra}$ : $^{224}\text{Ra}$  ratio observed at depth for USGT10-9 (0.18). While Mid Ocean Ridge Basalts (MORB) are generally enriched in  $^{231}\text{Pa}$  (relative to  $^{235}\text{U}$ ), they are only moderately so with activity ratios ( $^{231}\text{Pa}$ : $^{232}\text{Th}$ ) of 0.08-0.19 (Bourdon et al., 2000). Here they are  $\sim 6$ , which can only be explained by an additional benthic  $^{231}\text{Pa}$  or  $^{227}\text{Ac}$  source. One possibility is low temperature fluid circulation from the ridge similar to that proposed Moore et al. (2008) for the Puna Ridge. Alternatively, diffusion from metalliferous sediments at the base of the TAG hydrothermal mound may be providing the additional  $^{223}\text{Ra}$ . Support for this idea is detailed in German et al. (1993), who found excess  $^{231}\text{Pa}$  in metal-rich sediments at the base of the TAG mound, which they attributed to scavenging and removal from the overlying buoyant hydrothermal plume (German et al., 1991). Furthermore, as we will report in a follow-on paper,  $^{227}\text{Ac}$  is even further enriched over

$^{231}\text{Pa}$  in plume particles due to scavenging from a previously unrecognized deep ocean source of  $^{227}\text{Ac}$  originating from hydrothermal vents (Kipp et al., 2014). Once deposited, these  $^{227}\text{Ac}$ -rich sediments could supply significant activities of  $^{223}\text{Ra}$  to the benthic environment over hydrothermally-active ocean ridges. This process would be made possible due to the differential scavenging removal of Ac and Ra in the neutrally buoyant hydrothermal plume and a decoupling of Ac/Ra retention near field metalliferous sediments. Specifically, Lam et al. (2014) reported on the composition of particles in the plume sampled during GEOTRACES and found that 52% of the particle load (by weight) was comprised of Fe oxyhydroxides with no enrichment of Mn oxyhydroxides. While Ra isotopes have a well known affinity for Mn oxyhydroxides (Moore and Reid, 1973), their retention by Fe oxyhydroxides is quite poor (Krishnasawami et al., 1972). Hence, some fraction of the  $^{223}\text{Ra}$  produced by decay of  $^{227}\text{Ac}$  in the sediments would be available for release into the overlying water column.

#### 4. Conclusions

We presented the results of high resolution  $^{226}\text{Ra}$  and  $^{228}\text{Ra}$  measurements along the 2010-2011 U.S. GEOTRACES North Atlantic cruises. The large-scale distribution of  $^{226}\text{Ra}$  is reflective of the major water masses present in this region while  $^{228}\text{Ra}$  with its shorter half-life is a tracer of continental (upper ocean) and sedimentary (continental slope, deep ocean) sources. Deviations from the large scale features are due to Ra isotope inputs from the Mediterranean Outflow Water, hydrothermal vents from the TAG field or elevated benthic fluxes associated with lithogenic-rich sediments in the shadow of the Saharan dust plume. Follow-on papers will use the Ra isotopes to provide TEI rate processes such as benthic exchange, hydrothermal plume particle and mixing dynamics, and upper ocean mixing and transport.

Near the seafloor, pore water sources of dissolved TEIs can also be tracked by near bottom gradients in Ra (Sarmiento et al., 1982). In essence, concurrent measurement of Ra isotopes on the spatial resolution necessary to match that of GEOTRACES key TEIs allows one to quantify rates of key TEI input and transport processes with similar ocean boundary sources such as iron in Fe-limited ocean biomes (e.g. Windom et al., 2006; Charette et al., 2007; Dulaiova et al., 2009), manganese in oxygen minimum zones (e.g. Hatta et al., 2014), and cobalt along ocean margins (e.g. Noble et al., 2008). However, the importance of horizontal transport on Ra isotope distributions means that 1-D mixing models cannot adequately resolve vertical mixing rates through the thermocline or near the ocean bottom. More sophisticated 2-D or 3-D models will need to be developed in order to fully exploit the utility of these valuable ocean tracers.

#### Acknowledgements

The authors thank the chief scientists, captain, and crew of the *R/V Knorr* for all of their efforts in making the inaugural US GEOTRACES cruises a success. Sample collection and analyses were aided by members of the pumping group: Dan Ohnemus, Kuanbo Zhou, Stephanie Owens, Steve Pike, and Sylvain Rigaud. Dave Wellwood resurrected and repaired the 30-L Niskin bottles used to collect the small-volume  $^{226}\text{Ra}$  samples. Kanchan Maiti

provided access to his gamma counter on several occasions. Alan Shiller shared his barium data prior to its public release and the silicate analyses were performed by the Scripps Ocean Data Facility. This study was funded by the NSF Chemical Oceanography program (OCE-0925158 to M.A.C. and OCE-0926559 to W.S.M).

## References

- Armi, L. et al., 1989. 2 Years in the Life of a Mediterranean Salt Lens. *Journal of Physical Oceanography*, 19(3): 354-370.
- Bourdon, B., Goldstein, S.J., Bourles, D., Murrell, M.T. and Langmuir, C.H., 2000. Evidence from Be-10 and U series disequilibria on the possible contamination of mid-ocean ridge basalt glasses by sedimentary material. *Geochemistry Geophysics Geosystems*, 1.
- Broecker, W.S., 1979. Revised Estimate for the Radiocarbon Age of North-Atlantic Deep-Water. *Journal of Geophysical Research-Oceans and Atmospheres*, 84(Nc6): 3218-3226.
- Broecker, W.S., Goddard, J. and Sarmiento, J.L., 1976. Distribution of Ra-226 in Atlantic Ocean. *Earth and Planetary Science Letters*, 32(2): 220-235.
- Broecker, W.S., Li, Y.H. and Cromwell, J., 1967. Radium-226 and Radon-222 - Concentration in Atlantic and Pacific Oceans. *Science*, 158(3806): 1307-&.
- Chan, L.H. et al., 1976. Radium and Barium at Geosecs Stations in Atlantic and Pacific. *Earth and Planetary Science Letters*, 32(2): 258-267.
- Charette, M.A. et al., 2007. Radium isotopes as tracers of iron sources fueling a Southern Ocean phytoplankton bloom. *Deep-Sea Research Part II-Topical Studies in Oceanography*, 54(18-20): 1989-1998.
- Chung, Y., 1980. Radium-Barium-Silica Correlations and a Two-Dimensional Radium Model for the World Ocean. *Earth and Planetary Science Letters*, 49(2): 309-318.
- Chung, Y., Craig, H., Ku, T.L., Goddard, J. and Broecker, W.S., 1974. Radium-226 Measurements from 3 Geosecs Intercalibration Stations. *Earth and Planetary Science Letters*, 23(1): 116-124.
- Cochran, J.K. and Krishnaswami, S., 1980. Radium, Thorium, Uranium, and Pb-210 in Deep-Sea Sediments and Sediment Pore Waters from the North Equatorial Pacific. *American Journal of Science*, 280(9): 849-889.
- Deverdiere, A.C., 1992. On the Southward Motion of Mediterranean Salt Lenses. *Journal of Physical Oceanography*, 22(4): 413-420.
- Dulaiova, H., Ardelan, M.V., Henderson, P.B. and Charette, M.A., 2009. Shelf-derived iron inputs drive biological productivity in the southern Drake Passage. *Global Biogeochemical Cycles*, 23.
- German, C.R., Fleer, A.P., Bacon, M.P. and Edmond, J.M., 1991. Hydrothermal Scavenging at the Mid-Atlantic Ridge - Radionuclide Distributions. *Earth and Planetary Science Letters*, 105(1-3): 170-181.
- German, C.R. et al., 1993. A Geochemical Study of Metalliferous Sediment from the Tag Hydrothermal Mound, 26-Degrees-08'n, Mid-Atlantic Ridge. *Journal of Geophysical Research-Solid Earth*, 98(B6): 9683-9692.
- Hatta, M. et al., 2014. An overview of dissolved Fe and Mn Distributions during the 2010-2011 U.S. GEOTRACES north Atlantic Cruises: GEOTRACES GA03. *Deep Sea Research Part II: Topical Studies in Oceanography*(0).

- Hammond, D.E., Marton, R.A., Berelson, W.M. and Ku, T.L., 1990. Ra-228 Distribution and Mixing in San-Nicolas and San-Pedro Basins, Southern California Borderland. *Journal of Geophysical Research-Oceans*, 95(C3): 3321-3335.
- Hayes, C.T. et al., 2014.  $^{230}\text{Th}$  and  $^{231}\text{Pa}$  on GEOTRACES GA03, the U.S. GEOTRACES North Atlantic transect, and implications for modern and paleoceanographic chemical fluxes. *Deep Sea Research Part II: Topical Studies in Oceanography*(0).
- Henderson, P.B., Morris, P.J., Moore, W.S. and Charette, M.A., 2013. Methodological advances for measuring low-level radium isotopes in seawater. *Journal of Radioanalytical and Nuclear Chemistry*, 296(1): 357-362.
- Jenkins, W.J., Smethie Jr., W.M., Boyle, E.A. and Cutter, G.A., 2014. Water mass analysis for the U.S. GEOTRACES (GA03) North Atlantic Sections. *Deep Sea Research Part II: Topical Studies in Oceanography*, 0(0): 0.
- Jenkins, W.J., Lott III, D.E., Longworth, B.E., Curtice, J.M. and Cahill, K.L., 2014b. The distributions of helium isotopes and tritium along the U.S. GEOTRACES North Atlantic Sections. *Deep Sea Research Part II: Topical Studies in Oceanography*, 0(0): 0.
- Jickells, T.D. et al., 2005. Global iron connections between desert dust, ocean biogeochemistry, and climate. *Science*, 308(5718): 67-71.
- Kadko, D., 1996. Radioisotopic studies of submarine hydrothermal vents. *Reviews of Geophysics*, 34(3): 349-366.
- Kadko, D. and Moore, W., 1988. Radiochemical Constraints on the Crustal Residence Time of Submarine Hydrothermal Fluids - Endeavor Ridge. *Geochimica Et Cosmochimica Acta*, 52(3): 659-668.
- Kaufman, A., Trier, R.M., Broecker, W.S. and Feely, H.W., 1973. Distribution of Ra-228 in World Ocean. *Journal of Geophysical Research*, 78(36): 8827-8848.
- Key, R.M., Brewer, R.L., Stockwell, J.H., Guinasso, N.L. and Schink, D.R., 1979. Some Improved Techniques for Measuring Radon and Radium in Marine-Sediments and in Seawater. *Marine Chemistry*, 7(3): 251-264.
- Key, R. M., Moore, W. S. & Sarmiento, J. L. Transient Tracers in the Ocean North Atlantic Study Final Data Report for  $^{228}\text{Ra}$  and  $^{226}\text{Ra}$ ; Technical Report #92-2, Ocean Tracer Laboratory, Dept. Geology and Geophysics, Princeton University, Princeton, NJ, 193 pp. (1992).
- Key, R. M., Moore, W. S. & Sarmiento, J. L. Transient Tracers in the Ocean Tropical Atlantic Study Final Data Report for  $^{228}\text{Ra}$  and  $^{226}\text{Ra}$ , Technical Report #92-3, Ocean Tracer Laboratory, Dept. Geology and Geophysics, Princeton University, Princeton, NJ, 298 pp. (1992).
- Key, R. M., Rotter, R.J., McDonald, G.J. & Slater, R.D.. Western Boundary Exchange Experiment Final Data Report for large volume samples  $^{228}\text{Ra}$ ,  $^{226}\text{Ra}$ ,  $^9\text{Be}$ , and  $^{10}\text{Be}$  Results; Technical Report #90-1, Ocean Tracer Laboratory, Dept. Geology and Geophysics, Princeton University, Princeton, NJ, 298 pp. (1990).
- Kipp, L., Charette, M., Buesseler, K., Lam, P., Ohnemus, D., and Moore, W. 2014. Scavenging of Radionuclides and Elements in a Neutrally Buoyant Mid-Atlantic Ridge Hydrothermal Plume. *Mineralogical Magazine*, 77(5): 1264.
- Krishnasawmi, S., Lab, D., Somayajulu, B.L.K, Dixon, F.S., Stonecipher, S.A., and Craig, H. 1972. Silocon, radium, thorium, and lead in sea water: In-situ extraction by synthetic fiber. *Earth and Planetary Science Letters*, 16: 84-90.

- Krishnaswami, S., and Turekian, K.K. 1982.  $^{238}\text{U}$ ,  $^{226}\text{Ra}$ , and  $^{210}\text{Pb}$  in some vent waters of the Galapagos Spreading Center. *Geophysical Research Letters*, 9(8): 827-830.
- Ku, T.L. and Lin, M.C., 1976. Ra-226 Distribution in Antarctic Ocean. *Earth and Planetary Science Letters*, 32(2): 236-248.
- Ku, T.L. and Luo, S.D., 1994. New Appraisal of Ra-226 as a Large-Scale Oceanic Mixing Tracer. *Journal of Geophysical Research-Oceans*, 99(C5): 10255-10273.
- Kwon, E.Y., Kim, G., Primeau, F., Moore, W.S., Cho, H. - M., DeVries, T., Sarmiento, J.L., Charette, M.A. and Cho, Y. - K. 2014. Global estimate of submarine groundwater discharge based on an observationally constrained radium isotope model. *Geophys. Res. Lett.*, 41, doi:10.1002/2014GL061574.
- Lam, P.J., Ohnemus, D.C., and Auro, M.E. Size-fractionated major particle composition and concentrations from the US GEOTRACES north Atlantic zonal transect. *Deep Sea Research II*. DOI:/10.1016/j.dsr2.2014.11.020.
- Lam, P. J. and Morris, P. J. (pat. pending) In situ marine sample collection system and methods. 13/864,655.
- Measures, C., Hatta, M., Fitzsimmons, J. and Morton, P., 2014. Dissolved Al in the zonal N Atlantic section of the US GEOTRACES 2010/2011 cruises and the importance of Hydrothermal inputs. *Deep Sea Research Part II: Topical Studies in Oceanography*(0).
- Moore, W.S., 1969. Oceanic Concentrations of  $^{228}\text{Radium}$ . *Earth and Planetary Science Letters*, 6(6): 437-&.
- Moore, W.S., 1972. Ra-228 - Application to Thermocline Mixing Studies. *Earth and Planetary Science Letters*, 16(3): 421-446.
- Moore, W.S., and Reid, D.F., 1973. Extraction of Radium from Natural Waters Using Manganese-Impregnated Acrylic Fibers. *Journal of Geophysical Research*, 78(36): 8880-8886.
- Moore, W.S., 1984. Radium Isotope Measurements Using Germanium Detectors. *Nuclear Instruments & Methods in Physics Research Section a-Accelerators Spectrometers Detectors and Associated Equipment*, 223(2-3): 407-411.
- Moore, W.S., and R. Arnold, 1996. Measurement of  $^{223}\text{Ra}$  and  $^{224}\text{Ra}$  in coastal waters using a delayed coincidence counter. *J. Geophys. Res.*, 101(C1): 1321-1329.
- Moore, W.S. 1996. Large groundwater inputs to coastal waters revealed by  $^{226}\text{Ra}$  enrichments. *Nature*, 380: 612-614.
- Moore, W.S., 2000a. Determining coastal mixing rates using radium isotopes. *Cont. Shelf Res.*, 20: 1993-2007.
- Moore, W.S., 2000b. Ages of continental shelf waters determined from  $^{223}\text{Ra}$  and  $^{224}\text{Ra}$ . *J. Geophys. Res.*, 105(C9): 22,117-23,894.
- Moore, W.S., 2008. Fifteen years experience in measuring Ra-224 and Ra-223 by delayed-coincidence counting. *Marine Chemistry*, 109(3-4): 188-197.
- Moore, W.S., Astwood, H. and Lindstrom, C., 1995. Radium Isotopes in Coastal Waters on the Amazon Shelf. *Geochimica Et Cosmochimica Acta*, 59(20): 4285-4298.
- Moore, W.S. and Dymond, J., 1991. Fluxes of Ra-226 and Barium in the Pacific-Ocean - the Importance of Boundary Processes. *Earth and Planetary Science Letters*, 107(1): 55-68.
- Moore, W.S., Feely, H.W. and Li, Y.H., 1980. Radium Isotopes in Sub-Arctic Waters. *Earth and Planetary Science Letters*, 49(2): 329-340.

- Moore, W.S., Key, R.M. and Sarmiento, J.L., 1985. Techniques for Precise Mapping of Ra-226 and Ra-228 in the Ocean. *Journal of Geophysical Research-Oceans*, 90(Nc4): 6983-6994.
- Moore, W.S., Sarmiento, J.L. and Key, R.M., 2008. Submarine groundwater discharge revealed by Ra-228 distribution in the upper Atlantic Ocean. *Nature Geoscience*, 1(5): 309-311.
- Moore, W.S., Ussler, W. and Paull, C.K., 2008. Short-lived radium isotopes in the Hawaiian margin: Evidence for large fluid fluxes through the Puna Ridge. *Marine Chemistry*, 109(3-4): 421-430.
- Noble, A.E., Saito, M.A., Maiti, K. and Benitez-Nelson, C.R., 2008. Cobalt, manganese, and iron near the Hawaiian Islands: A potential concentrating mechanism for cobalt within a cyclonic eddy and implications for the hybrid-type trace metals. *Deep-Sea Research Part II-Topical Studies in Oceanography*, 55(10-13): 1473-1490.
- Peterson, R.N., Burnett, W.C., Dimova, N. and Santos, I.R., 2009. Comparison of measurement methods for radium-226 on manganese-fiber. *Limnology and Oceanography-Methods*, 7: 196-205.
- Rama and Moore, W.S., 1996. Using the radium quartet for evaluating groundwater input and water exchange in salt marshes. *Geochimica Et Cosmochimica Acta*, 60(23): 4645-4652.
- Rona, P.A. et al., 1984. Hydrothermal Activity at the Trans-Atlantic Geotraverse Hydrothermal Field, Mid-Atlantic Ridge Crest at 26-Degrees-N. *Journal of Geophysical Research*, 89(Nb13): 1365-1377.
- Rudnicki, M.D. and Elderfield, H., 1992. Helium, Radon and Manganese at the Tag and Snake-Pit Hydrothermal Vent Fields, 26-Degrees and 23-Degrees-N, Mid-Atlantic Ridge. *Earth and Planetary Science Letters*, 113(3): 307-321.
- Sarmiento, J.L., Rooth, C.G.H. and Broecker, W.S., 1982. Ra-228 as a Tracer of Basin Wide Processes in the Abyssal Ocean. *Journal of Geophysical Research-Oceans and Atmospheres*, 87(Nc12): 9694-9698.
- Sarmiento, J.L., Thiele, G., Key, R.M. and Moore, W.S., 1990. Oxygen and Nitrate New Production and Remineralization in the North-Atlantic Subtropical Gyre. *Journal of Geophysical Research-Oceans*, 95(C10): 18303-18315.
- Schmidt, S. and Reys, J.L., 1996. Radium as internal tracer of Mediterranean outflow water. *Journal of Geophysical Research-Oceans*, 101(C2): 3589-3595.
- Shiller, A.M. 2013. Dissolved Ga, Pb, and Ba from GEOTRACES Rosette bottles from GT10 and GT11 cruises. <http://www.bco-dmo.org/dataset/3827>
- Stakes, D. and Moore, W.S., 1991. Evolution of Hydrothermal Activity on the Juan-De-Fuca Ridge - Observations, Mineral Ages, and Ra Isotope Ratios. *Journal of Geophysical Research-Solid Earth*, 96(B13): 21739-21752.
- Trier, R.M., Broecker, W.S. and Feely, H.W., 1972. Ra-228 Profile at Second Geosecs Intercalibration Station, 1970, in North-Atlantic. *Earth and Planetary Science Letters*, 16(1): 141-&.
- Turekian, K.K. and Cochran, J.K., 1986. Flow-Rates and Reaction-Rates in the Galapagos Rise Spreading Center Hydrothermal System as Inferred from Ra-228/Ra-226 in Vesicomid Clam Shells. *Proceedings of the National Academy of Sciences of the United States of America*, 83(17): 6241-6244.
- van Beek, P. et al., 2007. Ra-228/Ra-226 and Ra-226/Ba ratios to track barite formation and transport in the water column. *Geochimica Et Cosmochimica Acta*, 71(1): 71-86.

Windom, H.L., Moore, W.S., Niencheski, L.F.H. and Jahrike, R.A., 2006. Submarine groundwater discharge: A large, previously unrecognized source of dissolved iron to the South Atlantic Ocean. *Marine Chemistry*, 102(3-4): 252-266.

ACCEPTED MANUSCRIPT

## Tables

Table 1. Relative parameters for measuring  $^{228}\text{Ra}$  by  $^{228}\text{Ac}$  or  $^{212}\text{Pb}$  (after  $^{228}\text{Th}$  ingrowth) via gamma spectroscopy. The detection factor is equal to the inverse of the product of detector efficiency, including self absorption in the sample matrix (E) and peak intensity (I). A lower factor will result in more intense peak on the gamma spectrum and therefore a higher probability of detection and lower analytical uncertainties for the same counting period and sample count rate.

Radionuclide	energy (keV)	I (peak intensity)	E (relative efficiency)	Factor
$^{228}\text{Ac}$	338	0.114	0.26	33.3
$^{228}\text{Ac}$	911	0.277	0.08	45.3
$^{212}\text{Pb}$	238	0.423	0.43	5.5

Table 2. Comparison of  $15^\circ \times 15^\circ$  box average inventories (full water column) of  $^{226}\text{Ra}$  ( $\times 10^{13}$  atoms  $\text{m}^{-2}$ ) for samples collected on the GEOTRACES Atlantic section (2010-2011) and the Transient Tracers in the Ocean cruises (1981-1986). Errors are the standard deviation of values in each box. There was only one GEOTRACES station in box 3.

GEOTRACES Atlantic section	Transient Tracers in the Ocean
10.7 $\pm$ 0.8	11.3 $\pm$ 0.6
10.6 $\pm$ 0.8	10.4 $\pm$ 0.6
(10.9)	10.4 $\pm$ 0.3
10.4 $\pm$ 0.4	10.9 $\pm$ 0.9
10.8 $\pm$ 0.3	11.1 $\pm$ 0.6
11.6 $\pm$ 0.5	11.6 $\pm$ 0.8
Total 65.0 $\pm$ 1.3	Total 65.7 $\pm$ 1.6

Table 3. Comparison of box average upper ocean (0-1000 m) inventories of  $^{228}\text{Ra}$  ( $\times 10^{10}$  atoms  $\text{m}^{-2}$ ) for samples collected on the GEOTRACES Atlantic section (2010-2011) and the Transient Tracers in the Ocean cruises (1981-1986). Errors are the standard deviation of values in each box. There was only one GEOTRACES station in box 3. The number in parenthesis is inflated due to a deep component of high  $^{228}\text{Ra}$  Mediterranean Outflow Water. Data are also shown in Figure 9.

GEOTRACES Atlantic section	Transient Tracers in the Ocean
5.9 $\pm$ 1.3	5.4 $\pm$ 1.5
3.8 $\pm$ 0.9	4.1 $\pm$ 0.5
(4.6)	3.5 $\pm$ 0.9
4.4 $\pm$ 0.3	4.0 $\pm$ 1.0
3.4 $\pm$ 0.5	3.6 $\pm$ 0.8
2.5 $\pm$ 0.8	2.4 $\pm$ 0.4
Total 24.6 $\pm$ 1.9	Total 22.9 $\pm$ 2.3

## Figures

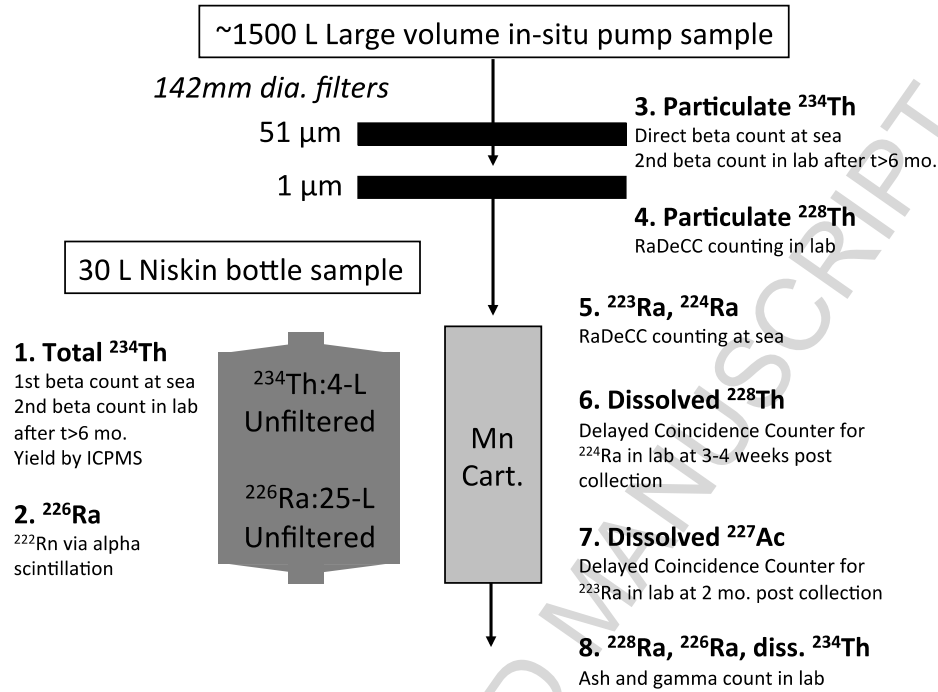


Figure 1. Flow chart illustrating sample collection and processing procedures for Ra and Th isotope determination on the GEOTRACES North Atlantic Zonal Transect cruises.

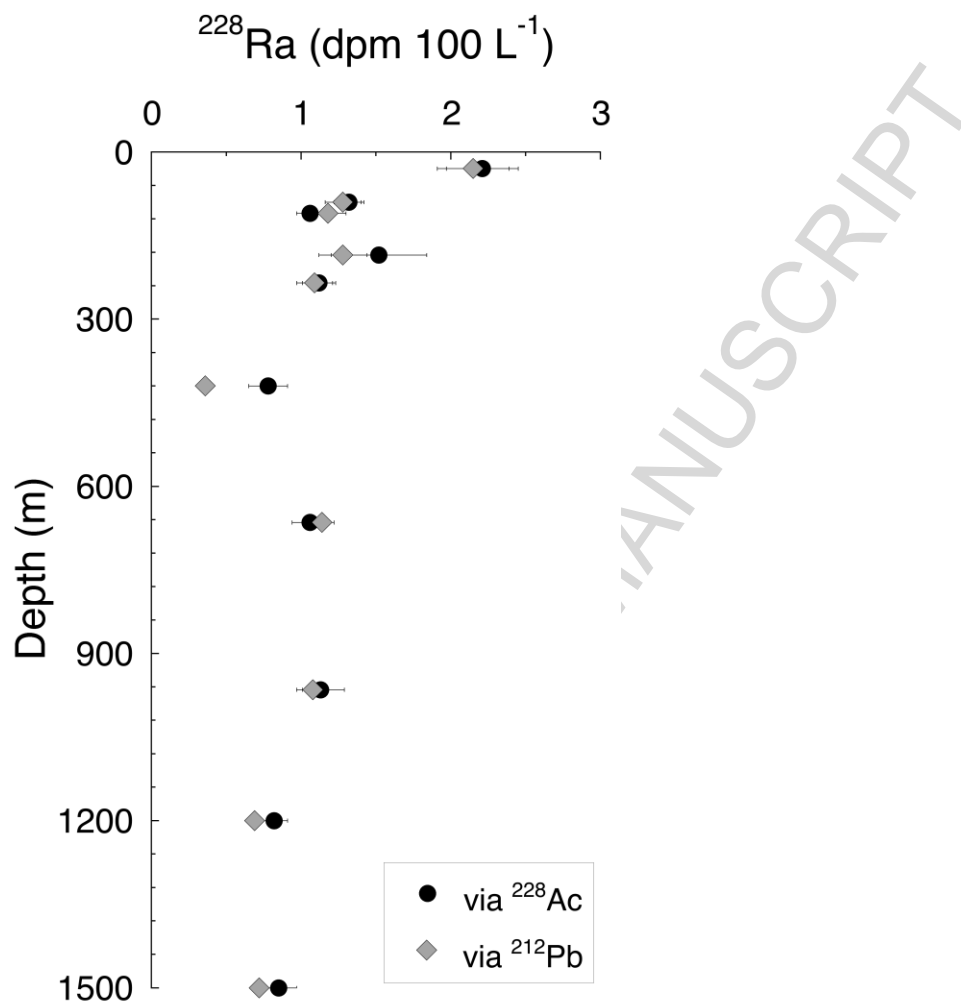


Figure 2. Comparison of  $^{228}\text{Ra}$  determination by gamma counting using the  $^{228}\text{Ac}$  daughter photopeak (338 or 911 keV) or  $^{212}\text{Pb}$  (238 keV) for station USGT10-1.

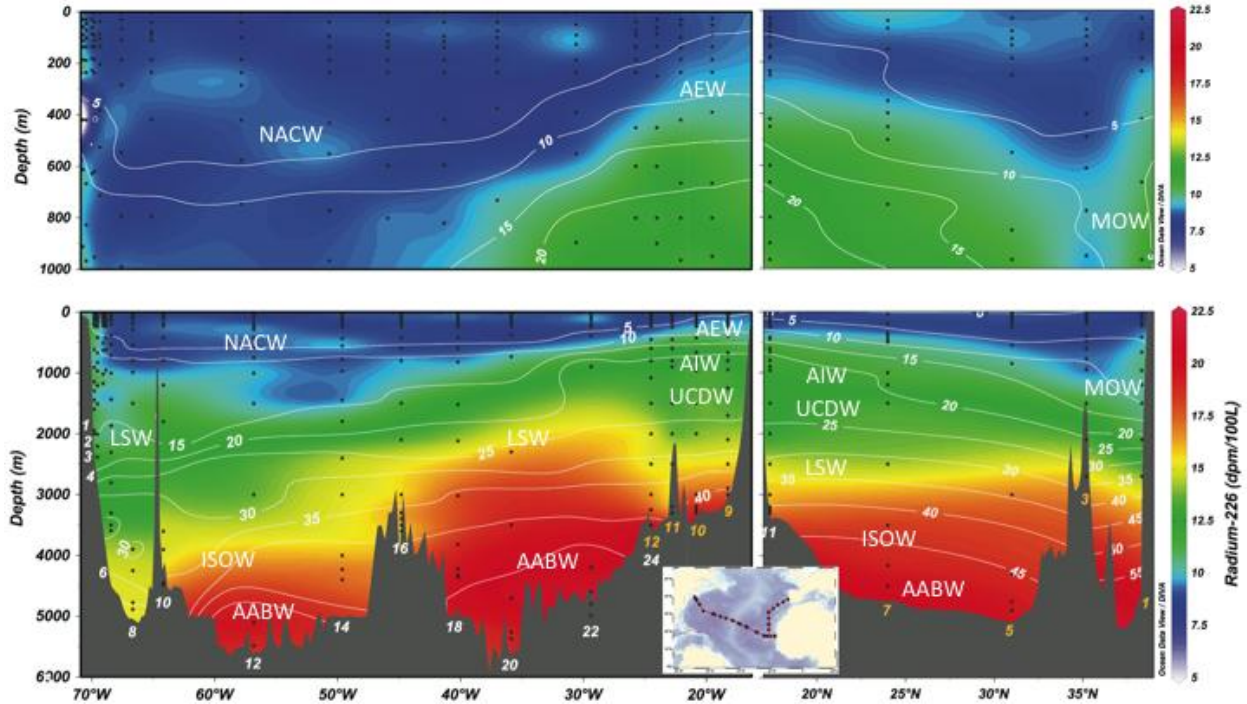


Figure 3. Radium-226 distribution (dpm/100 L) along the USGT10 & USGT11 cruise tracks. The left panels are the zonal transect while the right panels are the meridional transect. Station numbers for USGT10 (yellow) and USGT11 (white) are shown along the illustrated seafloor. All panels are overlain with silicate concentrations ( $\mu\text{M}$ ; white contour lines and labels) and the location of major water masses as reported in Jenkins et al. (2014). Water mass abbreviations are as follows: North Atlantic Central Water (NACW), Atlantic Equatorial Water (AEW), Labrador Sea Water (LSW), Antarctic Intermediate Water (AIW), Upper Circumpolar Deep Water (UCDW), Iceland Scotland Overflow Water (ISOW), Antarctic Bottom Water (AABW), and Mediterranean Outflow Water (MOW).

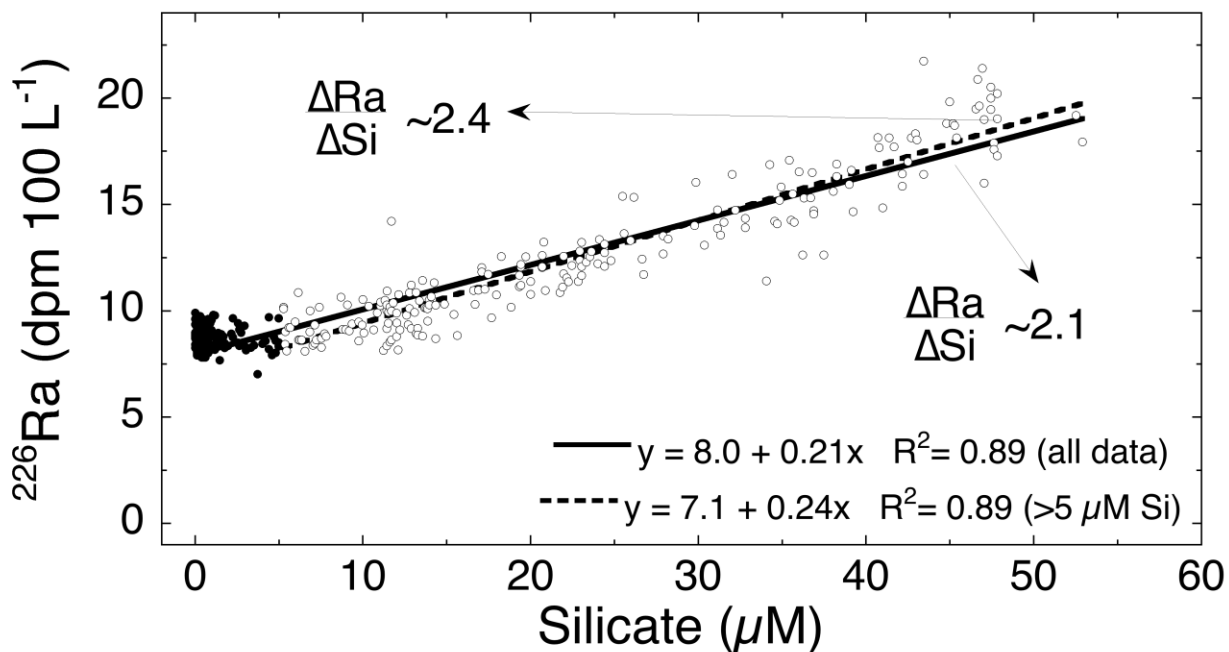


Figure 4. Radium-226/silicate relationship for US GEOTRACES North Atlantic. The reported Ra/Si ratios have units of  $10^3\text{dpm/mol}$ . The solid line is the curve fit for all samples ( $R^2=0.89$ ) while the dashed line is for only samples with silicate  $> 5 \mu\text{M}$  ( $R^2=0.89$ ).

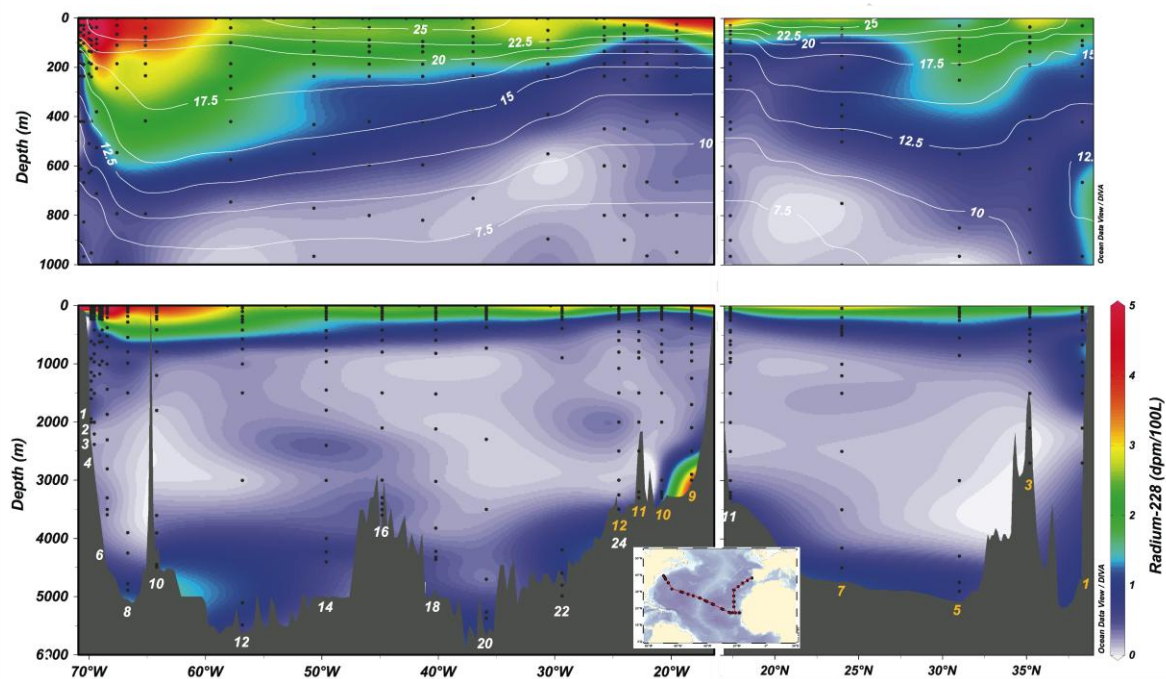


Figure 5. Radium-228 distribution (dpm/100 L) along the USGT10 & USGT11 cruise tracks. The left panels are the zonal transect while the right panels are the meridional transect. The upper panels are overlain with potential temperature ( $^{\circ}\text{C}$ ; white contour lines and labels).

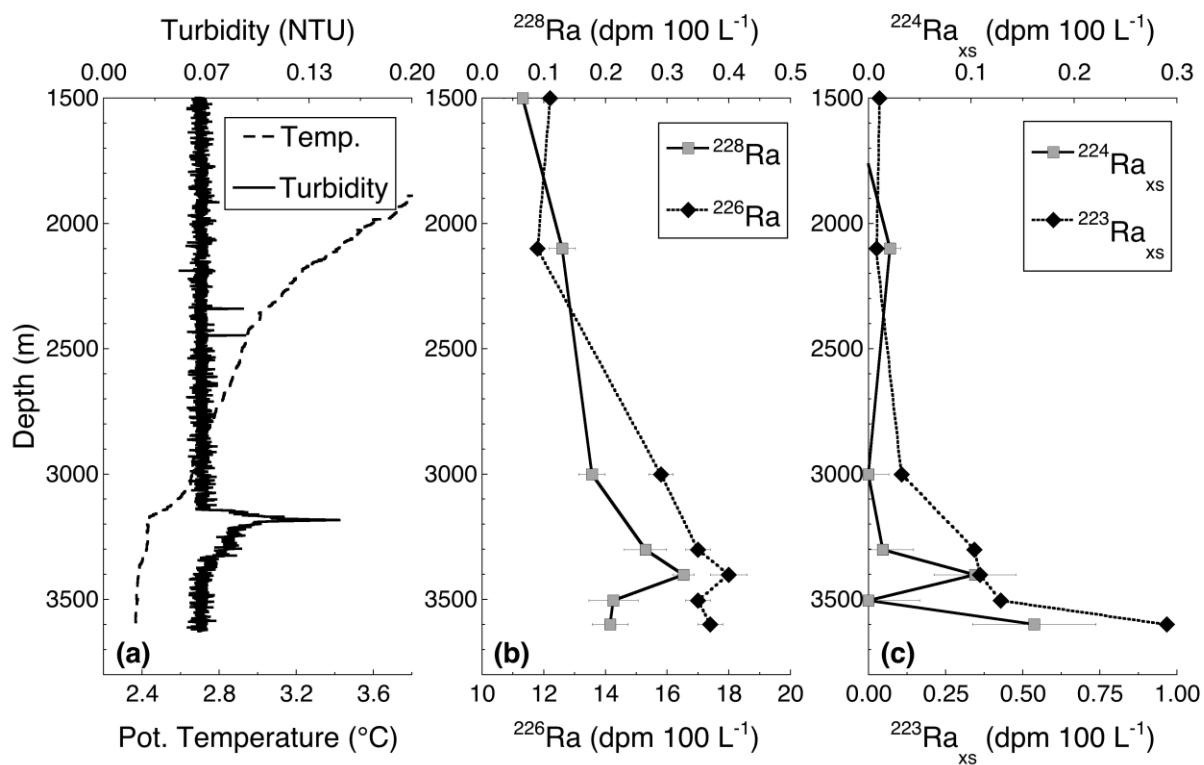


Figure 6. Radium isotope distributions in the lower water column at station USGT11-16 (TAG hydrothermal plume). Panel (a) turbidity and potential temperature, (b)  $^{226}\text{Ra}$  and  $^{228}\text{Ra}$ , and (c)  $^{223}\text{Ra}_{\text{XS}}$  and  $^{224}\text{Ra}_{\text{XS}}$ .

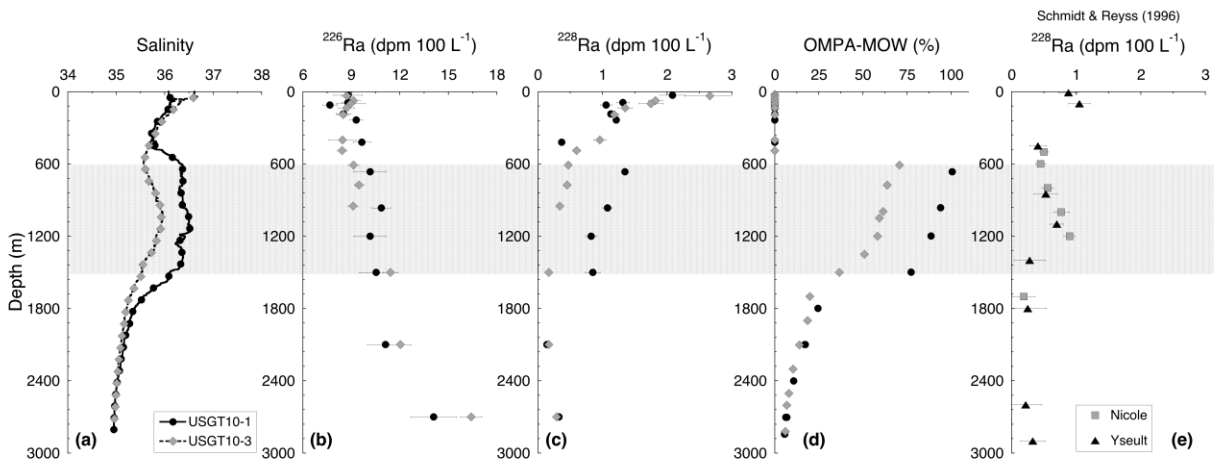


Figure 7. Mediterranean Outflow Stations (USGT10-1 and USGT10-3) (a) salinity, (b)  $^{226}\text{Ra}$ , (c)  $^{228}\text{Ra}$ , (d) fraction of MOW derived from the OMPA analysis of Jenkins et al. (2014), and (e)  $^{228}\text{Ra}$  from MOW eddies in 1989 as reported by Schmidt and Reyss (1996). The core of the MOW plume is indicated by the grey shading.

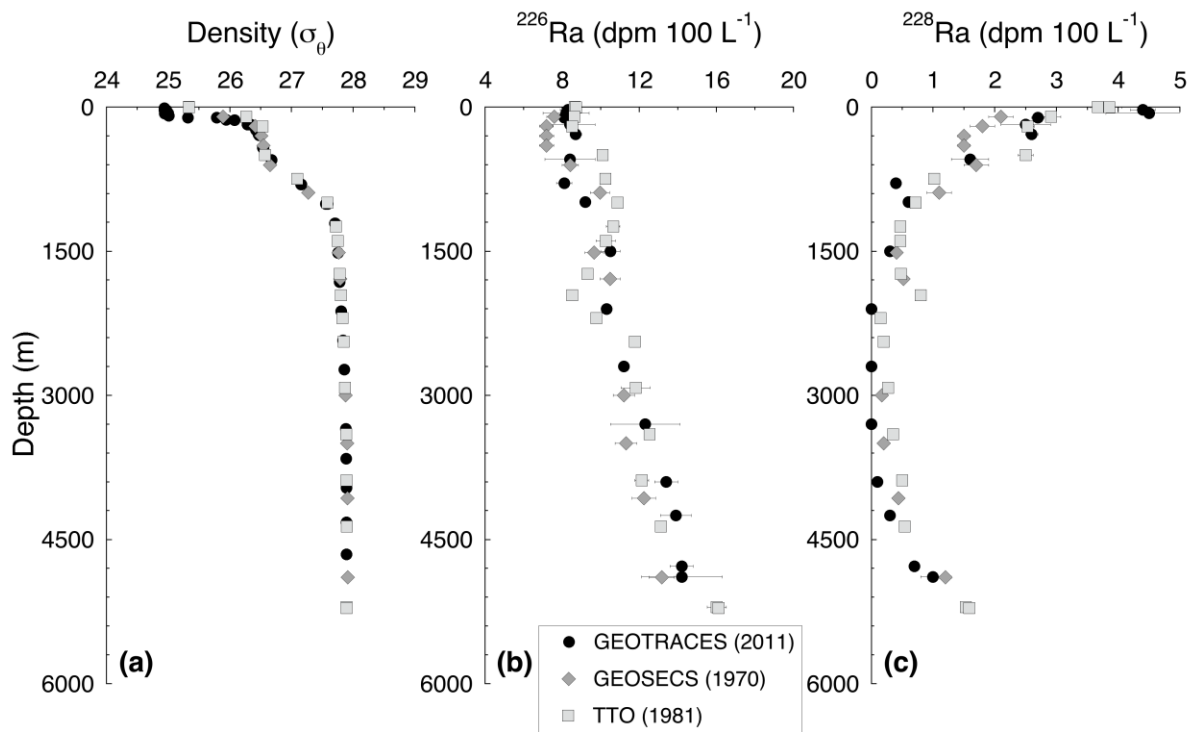


Figure 8. Comparison of Ra isotopes at USGT11-8 with proximal GEOSECS and TTO stations. Panel (a) shows density, (b)  $^{226}\text{Ra}$ , and (c)  $^{228}\text{Ra}$ . Error bars may be smaller than the symbols in some cases.

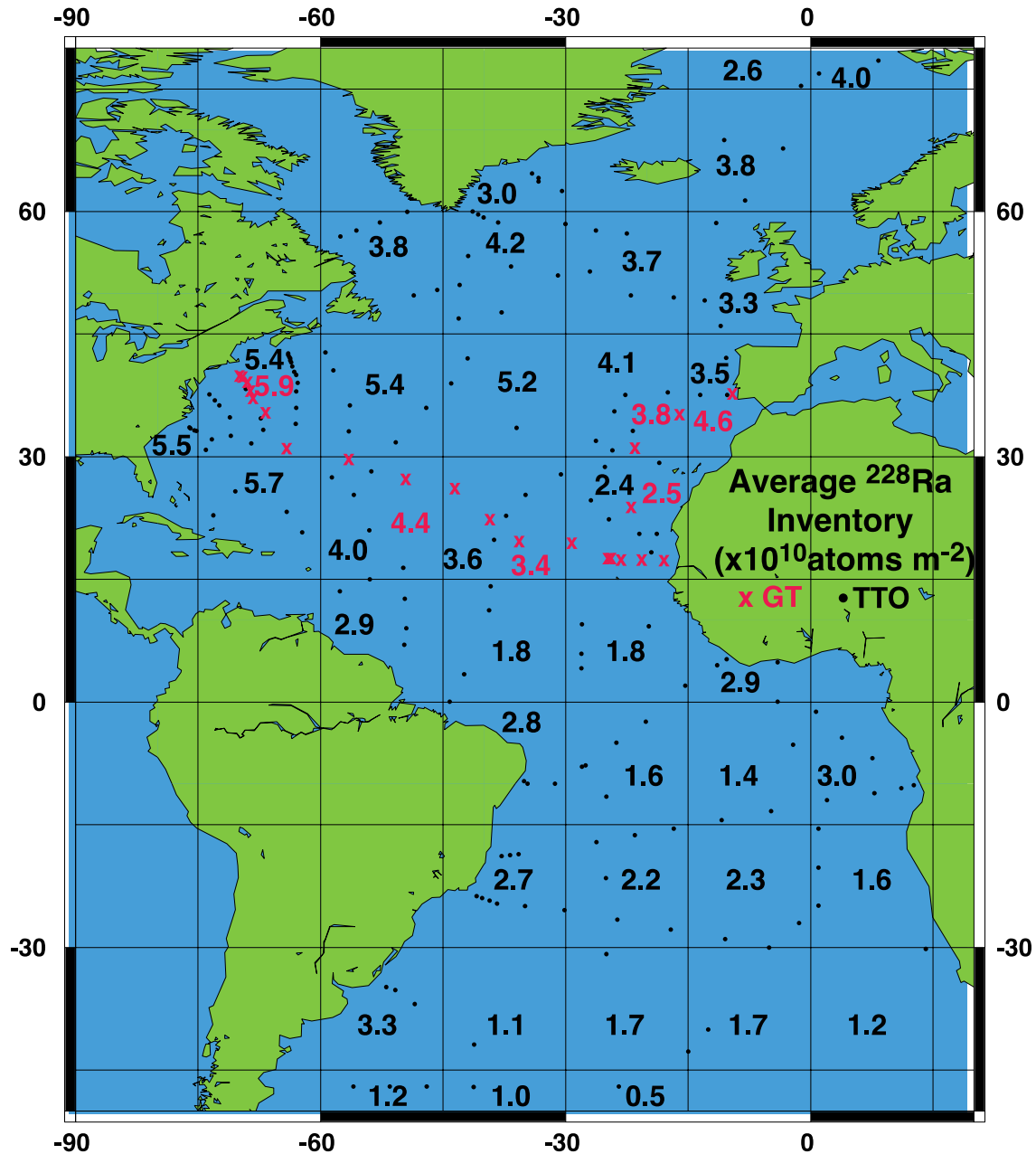


Figure 9. Box average 0-1000 m inventories ( $15^\circ \times 15^\circ$ ) of  $^{228}\text{Ra}$  ( $\times 10^{10}$  atoms  $\text{m}^{-2}$ ) for samples collected on the GEOTRACES Atlantic section (GT) (2010-2011) and the Transient Tracers in the Ocean cruises (TTO) (1981-1986). Each solid black dot is a TTO station, each red x is a GT station.

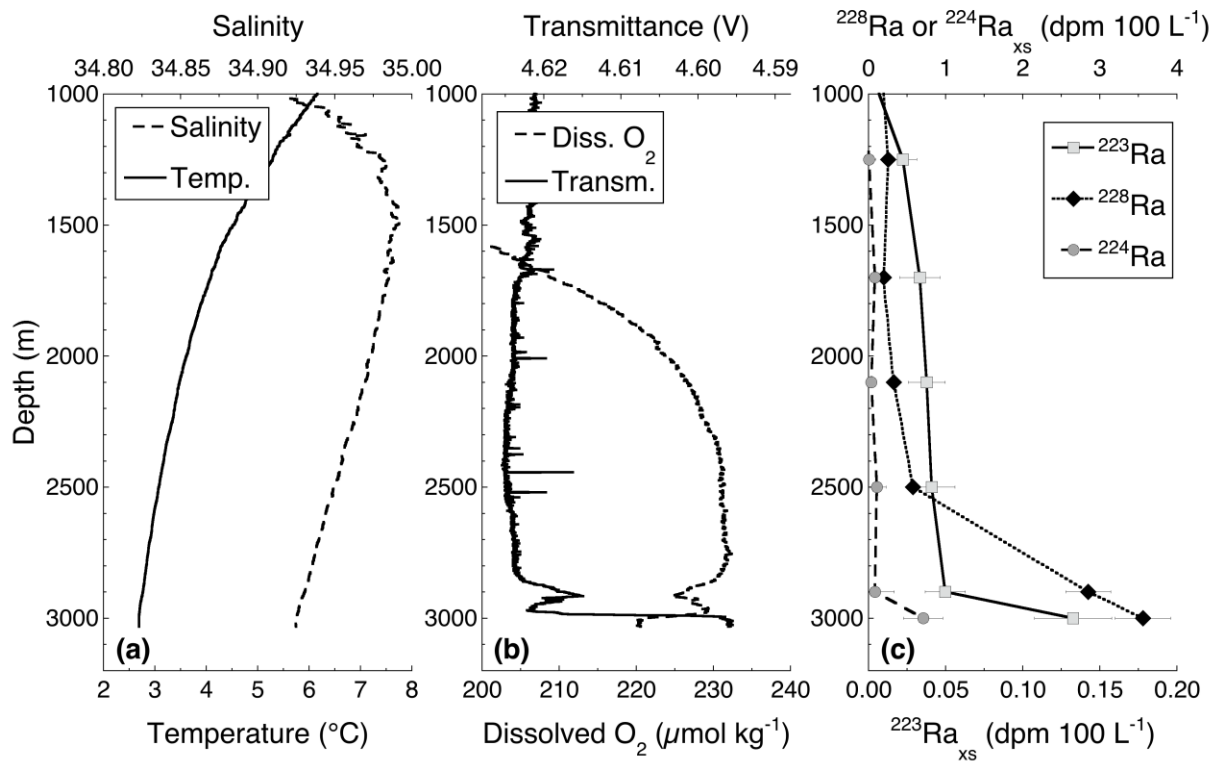


Figure 10. Mauritanian Upwelling Zone station USGT10-9 (a) salinity/temperature, (b) transmittance/dissolved oxygen, and (c)  $^{223}\text{Ra}_{\text{xs}}/^{228}\text{Ra}/^{224}\text{Ra}_{\text{xs}}$ . The transmittance is plotted on a reverse scale so that high values indicate higher particle concentrations.

Highlights for Charette et al. (2014)

- Benthic radium isotope fluxes are highest beneath the west African upwelling zone
- Mediterranean outflow transport rate of 0.5-0.8 cm/s quantified using  $^{228}\text{Ra}$
- Enhanced  $^{223}\text{Ra}$  fluxes from Mid-Atlantic Ridge sediments
- Elevated radium isotopes observed in a neutrally buoyant hydrothermal plume
- Atlantic Ocean submarine groundwater discharge is at steady-state over 40 years

ACCEPTED MANUSCRIPT